

## Article

# Jointly Active/Passive Beamforming Optimization for Intelligent-Reflecting Surface-Assisted Cognitive-IoT Networks

Yanping Zhou <sup>1</sup>, Fang Deng <sup>1,\*</sup> and Shidang Li <sup>2</sup>

<sup>1</sup> School of Internet of Things and Artificial Intelligence, Wuxi Vocational College of Science and Technology, Wuxi 214121, China; zyp@wxsc.edu.cn

<sup>2</sup> School of Physics and Electronic Engineering, Jiangsu Normal University, Xuzhou 221116, China; shidangli@jsnu.edu.cn

\* Correspondence: dengf@wxsc.edu.cn

**Abstract:** To overcome challenges such as limited energy availability for terminal devices, constrained network coverage, and suboptimal spectrum resource utilization, with the overarching objective of establishing a sustainable and efficient interconnection infrastructure, we introduce an innovative Intelligent Reflective Surface (IRS) technology. This cutting-edge IRS technology is employed to architect a wireless and energy-efficient cognitive secure communication network assisted by IRS. To further optimize the overall energy harvesting of this network, we present a cognitive secure resource allocation scheme, aiming to maximize the system's total collected energy. This scheme carefully considers various constraints, including transmission power constraints for cognitive base stations, power constraints for jammer devices, interference limitations for all primary users, minimum security rate constraints for all cognitive Internet of Things (IoT) devices, and phase shift constraints for IRS. We establish a comprehensive hybrid cognitive secure resource allocation model, encompassing joint cognitive transmission beam design, jammer device transmission beam design, and phase shift design. Given the non-convex nature of the formulated problem and the intricate coupling relationships among variables, we devise an effective block coordinate descent (BCD) iterative algorithm. The realization of joint cognitive/jammer base station transmission beam design and phase shift design employs sophisticated techniques such as continuous convex approximation methods and semi-definite programming. Simulation results underscore the superior performance of the proposed scheme compared to existing resource allocation approaches, particularly in terms of total harvested energy and other critical metrics.

**Keywords:** spectrum resource utilization; intelligent reflecting surfaces; energy harvesting; security rate; block coordinate descent



**Citation:** Zhou, Y.; Deng, F.; Li, S. Jointly Active/Passive Beamforming Optimization for Intelligent-Reflecting Surface-Assisted Cognitive-IoT Networks. *Electronics* **2024**, *13*, 299. <https://doi.org/10.3390/electronics13020299>

Academic Editor: Domenico Ursino

Received: 3 December 2023

Revised: 25 December 2023

Accepted: 3 January 2024

Published: 9 January 2024



**Copyright:** © 2024 by the authors. Licensee MDPI, Basel, Switzerland. This article is an open access article distributed under the terms and conditions of the Creative Commons Attribution (CC BY) license (<https://creativecommons.org/licenses/by/4.0/>).

## 1. Introduction

The proliferation of Internet of Things (IoT) devices globally, including smartphones, tablets, various sensors, and wearable devices, is projected to increase from 7 billion to 22 billion, laying the foundation for a pervasive connectivity paradigm in the future [1,2]. However, over the past decades, a significant portion of the available spectrum has been allocated primarily to high-speed communication services, resulting in a scarcity of spectrum resources within wireless communication systems. Conversely, the efficiency of utilizing the abundant spectrum remains suboptimal. Cognitive radio (CR) emerges as an innovative approach to address the scarcity of spectrum resources [3–8]. In CR networks, cognitive users (CUs) are authorized to use frequency bands designated for primary users (PUs) for communication, ensuring minimal interference to PUs. The interference generated by CUs, affecting PUs, is commonly referred to as interference temperature. Network security is a critical concern in CR networks [9–12]. Due to the intrinsic broadcast properties of wireless communication, transmission information is vulnerable to interception by unauthorized

users. In the past, security challenges in wireless networks were predominantly addressed by encrypting transmission signals using secret keys. However, certain security challenges persisted, such as the key allocation problem in symmetric cryptosystems and the high complexity problem in asymmetric cryptosystems. In recent years, physical layer security (PLS) technology has emerged as a promising alternative or complement to encryption technology, with researchers developing various approaches to enhance the PLS of wireless networks [13–15]. Multiple-antenna technology, considered pivotal in the realm of future wireless communication, has the potential to significantly enhance the security rate of wireless communication. Moreover, the strategic introduction of artificial noise to the transmission signal at a specific power level proves to be an effective strategy to interfere with the signal reception of eavesdropping users, thereby enhancing communication security [16].

The rapid expansion of large-scale IoT applications has notably augmented the power consumption of wireless devices. In addressing this, a comprehensive massive access scheme for 6G cellular IoT was proposed in [17], aiming to facilitate efficient massive access while enhancing energy efficiency within the constraints of limited spectrum resources, while the authors in [18] have put forth an AI-based adaptive security specification approach to tackle the elevated energy (EE) consumption resulting from advanced security measures for IoT devices. This approach tailors security specifications to corresponding business requirements, mitigating energy depletion concerns and extending operational time. Despite these advancements, ensuring a sustainable energy supply for a vast array of IoT devices remains a formidable challenge. The utilization of wired power supply for IoT devices is impractical for large-scale deployment, and the energy storage capacity of battery power is inherently limited, posing constraints on the sustained operation of the entire IoT ecosystem [19]. Although the replacement of batteries can alleviate the energy shortage issue, the environmental limitations associated with the large-scale deployment of IoT devices contribute to high operational costs [20].

Wireless power transfer (WPT) has become a focal point of attention in both academic and industrial circles, emerging as a dependable solution for powering IoT devices in recent years [21–23]. Reference [21] introduces a theoretical framework tailored for 6G cellular IoT, emphasizing the integration of energy, computation, and communication aspects. The authors investigate the potential of utilizing WPT to establish a sustainable power supply for a diverse array of IoT devices. They propose a joint beamforming design scheme for both the transmitter and receiver to optimize EE. In the context of remote WPT, the literature [22] puts forth a resonant beam charging method. This method facilitates the simultaneous transmission of wireless signals and energy, defining one of the applications of WPT technology known as Wireless Energy and Information Transmission (WEIT). Specifically, Simultaneous Wireless Information and Power Transfer (SWIPT), a form of WPT incorporating bi-directional energy exchange, is explored in the literature [23]. The study focuses on an SWIPT system with full-duplex IoT nodes, proposing an optimization scheme for joint hybrid precoding, decoding rules, and power allocation to minimize total transmission power. Therefore, leveraging the dual nature of wireless signals that encompass both information and energy, SWIPT technology holds the promise of achieving a sustainable power supply and efficient communication for IoT devices simultaneously, aligning with the fundamental requirements of green communication for the new generation of IoT.

On the contrary, the emerging IRS technology [24–27] is considered a promising candidate for 6G systems. Essentially, IRS embodies a uniform array plane featuring a multitude of cost-effective, sub-wavelength, and autonomously adjustable passive electromagnetic reflecting elements. These elements provide the capability to precisely manipulate the amplitude and phase of reflected signals via software programming, utilizing feedback from the signal propagation data within the communication link. This dynamic capability enables the coherent superposition of the reflected signal with contributions from other transmission paths, thereby amplifying the power of the desired signal at the receiver and concurrently enhancing the overall communication quality [25–27]. In [28], a beamforming

design method is proposed based on the maximum–minimum criterion, jointly designing the beamformer of the Base Station (BS) and the IRS reflection phase shift to maximize the minimum harvested energy for an IRS-aided SWIPT system. Additionally, Ref. [29] examines an IRS-enabled MISO system with SIWPT. It presents an iterative algorithm for designing the transmit/reflection beamforming, aiming to maximize the weighted sum power of the energy-harvesting receiver (EHR).

Active and passive mutual transmission technology based on IRS is one of the promising physical layer solutions for 6G and IoT systems. However, this technology also raises PLS concerns [30–34]. In the work presented by [30], an iterative methodology augmented via the introduction of AN is introduced. The primary objective of this approach is to enhance energy efficiency within an IRS-aided SWIPT system, particularly considering a non-linear EH model. Furthermore, as delineated in [31], an alternating iterative algorithm rooted in Semi-Definite Relaxation (SDR) is advanced. This algorithm is dedicated to the minimization of transmit power within an IRS-assisted MIMO secure transmission system, simultaneously yielding a closed-form expression for secure beamforming. Moreover, this contribution significantly amplifies the overall effectiveness of the power allocation scheme. In [32], an iterative method combining the barrier method and item-by-item optimization was proposed to improve the secure rate in an IRS-enabled Gaussian MIMO system, where the CSI of the eavesdropper remains undisclosed. To achieve secrecy and rate maximization in a distributed IRS-assisted multi-user MIMO transmission system, ref. [33] proposed a joint optimization strategy of the penalty function method, SCA, and SDR to design a robust beamforming and AN scheme, considering the scenario where the eavesdropper's CSI is unknown and there is no LoS link. However, the interference techniques [34] that can effectively enhance the secure rate and energy transmission have not been investigated in the aforementioned literature. Furthermore, ref. [25–27] only addressed the IRS-assisted SWIPT system model, and [30–34] primarily focused on traditional secure transmission systems. The IRS-assisted SWIPT-CR communication system based on external interference technology can enhance the system's energy harvesting capability while improving communication security by emitting interference signals to counter eavesdropping.

In light of the challenges associated with energy transfer and information security mentioned earlier, the study of the PLS problem within a cognitive SWIPT system, with the assistance of IJ and IRS, bears both theoretical and practical importance. This paper makes specific contributions to the research in the following areas:

- In a cognitive SWIPT IoT system, we establish a secure communication link that receives simultaneous assistance from IJ and IRS. The EHR model is formulated by collaboratively optimizing the SBS beamforming matrix, the IJ's beamformer, and the phase shifts associated with the IRS. The central challenge lies in solving a non-convex quadratic optimization problem subject to quadratic constraints, which presents inherent difficulty.
- A novel alternate secure transmission algorithm is posed to address the aforementioned non-convex quadratic programming problem. First, the non-convex security constraint is transformed into a convex one by applying sequential parametric convex approximation (SPCA). Then, the initial non-convex objective function is approximated into a convex form by employing a first-order Taylor expansion, relaxation variables, SDR, and auxiliary variables. Finally, an alternating scheme rooted in SDR is devised to attain a viable solution for the initial non-convex conundrum.
- The simulation results offer compelling evidence of the algorithm's convergence, while also vividly demonstrating the substantial improvements in harvested energy realized by the cognitive SWIPT IoT system in the presence of IRS support. Compared with conventional schemes, the use of IRS offers significant advantages in enhancing system security and energy harvesting performance.

## 2. Network Model

Figure 1 depicts a model of a SWIPT cognitive IoT system assisted by IRS. The system comprises a multi-antenna SBS;  $K$  legitimate cognitive IoT devices, each with a single antenna;  $L$  eavesdropping devices (Eve); and  $P$  PUs. Given that Eves are assumed to be in closer proximity to the SBS than the IoT devices, they are better situated to eavesdrop on external information. It is reasonable to regard Eves as potential eavesdropping devices due to the importance of ensuring information security during transmission. To improve information transmission security,  $J$  EHRs are deployed near the IRS to collect radio frequency signal energy. Additionally, a jammer is utilized to emit interference signals. We make the assumption that both the SBS and the IJ are outfitted with  $M$  antennas, whereas the IRS is furnished with  $N$  reflection units. This system revolves around the conventional downlink transmission scenario from the SBS to the receiving device, with the additional assumption that the location of Eve can be ascertained using parameters such as AoA, RSS, TDoA, and ToA.

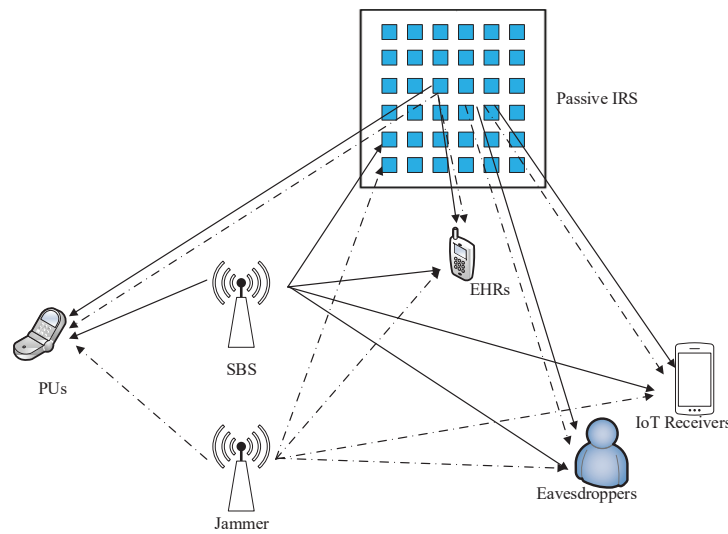


**Figure 1.** Illustration of an IRS-SWIPT-enabled Secure Transmission CR-IoT Network.

To achieve secure transmission of a SWIPT-enabled CR-IoT system in the presence of MIMO eavesdropping channels, we make the assumption that the channel gains linking the SBS with the IRS, the  $k$ -th IoT device, the  $j$ -th EHR, the  $l$ -th eavesdropper, and the  $p$ -th PU, which are denoted by  $\mathbf{H}_{BI} \in \mathbb{C}^{N \times M}$ ,  $\mathbf{h}_{BU,k} \in \mathbb{C}^{M \times 1}$ ,  $\mathbf{h}_{BEH,j} \in \mathbb{C}^{M \times 1}$ ,  $\mathbf{h}_{BEVE,l} \in \mathbb{C}^{M \times 1}$ , and  $\mathbf{h}_{BP,p} \in \mathbb{C}^{M \times 1}$ , respectively. The channel gains between the jammer and the IRS, the  $k$ -th IoT device, the  $j$ -th EHR, the  $l$ -th eavesdropper, and the  $p$ -th PU are denoted by  $\mathbf{G}_{JI} \in \mathbb{C}^{N \times M}$ ,  $\mathbf{g}_{JU,k} \in \mathbb{C}^{M \times 1}$ ,  $\mathbf{g}_{JEH,j} \in \mathbb{C}^{M \times 1}$ ,  $\mathbf{g}_{JEVE,l} \in \mathbb{C}^{M \times 1}$ , and  $\mathbf{g}_{JP,p} \in \mathbb{C}^{M \times 1}$ , respectively. Assuming that the IRS reflects signals from the SBS to the  $k$ -th IoT device, the  $j$ -th EHR, the  $l$ -th eavesdropper, and the  $p$ -th PU, their corresponding channel gains are represented by  $\mathbf{h}_{IU,k} \in \mathbb{C}^{N \times 1}$ ,  $\mathbf{h}_{IEH,j} \in \mathbb{C}^{N \times 1}$ ,  $\mathbf{h}_{IEVE,l} \in \mathbb{C}^{N \times 1}$ , and  $\mathbf{h}_{IP,p} \in \mathbb{C}^{N \times 1}$ , respectively. Additionally, we assume that the IRS reflects signals from the jammer to the same set of receivers, namely the  $k$ -th IoT device, the  $j$ -th EHR, the  $l$ -th Eve, and the  $p$ -th PU, and the corresponding channel gains are denoted by  $\mathbf{g}_{IU,k} \in \mathbb{C}^{N \times 1}$ ,  $\mathbf{g}_{IEH,j} \in \mathbb{C}^{N \times 1}$ ,  $\mathbf{g}_{IEVE,l} \in \mathbb{C}^{N \times 1}$ , and  $\mathbf{g}_{IP,p} \in \mathbb{C}^{N \times 1}$ , respectively. The IRS fine tunes the phase adjustments of its reflective elements to enhance the composite signal arriving at the user group. The diagonal phase shift matrix of the IRS is represented by  $\Theta = \text{diag}(e^{j\theta_1}, e^{j\theta_2}, \dots, e^{j\theta_N})$ , with the main diagonal corresponding to the phase shift of the  $n$ -th element of the composite incident signal,  $\forall n = 1, 2, \dots, N$ . Assuming ideal CSI and a quasi-static flat fading model for the channel gains across all connections, the transmission signal of the SBS and jammer can be represented as  $\mathbf{x}_1 = \sum_{k=1}^K f_k s_k$  and  $\mathbf{x}_2 = \mathbf{w}z$ , where the variables  $s_k$  and  $z$  are considered as complex Gaussian random variables which are independently and identically distributed. Although the CSI is imperfect in practical systems, ref. [35] proposed a novel

approach to successfully solve the channel estimation problem in a multi-user IRS system. Thus, we assume perfect CSI for the design of resource allocation in this paper. Meanwhile, the vectors  $f_k$  and  $w$  correspond to the beamforming of the  $k$ -th cognitive IoT device and jamming precoding vectors, respectively. The received signal related to the  $k$ -th cognitive IoT devices,  $l$ -th eavesdropper,  $j$ -th EHR, and  $p$ -th PU can be modeled as

$$y_{SU,k} = \sum_{i=1}^K (h_{BU,k}^H + h_{IU,k}^H \Theta H_{BI}) f_i s_i + (g_{JU,k}^H + g_{IU,k}^H \Theta G_{JI}) w z + n_{SU,k} \tag{1}$$

$$y_{SEV,l} = \sum_{i=1}^K (h_{BEVE,l}^H + h_{IEVE,l}^H \Theta H_{BI}) f_i s_i + (g_{JEVE,l}^H + g_{IEVE,l}^H \Theta G_{JI}) w z + n_{SEVE,l} \tag{2}$$

$$y_{SEH,j} = \sum_{i=1}^K (h_{BEH,j}^H + h_{IEH,j}^H \Theta H_{BI}) f_i s_i + (g_{JEH,j}^H + g_{IEH,j}^H \Theta G_{JI}) w z + n_{SEH,j} \tag{3}$$

$$y_{P,p} = \sum_{i=1}^K (h_{BP,p}^H + h_{IP,p}^H \Theta H_{BI}) f_i s_i + (g_{JP,p}^H + g_{IP,p}^H \Theta G_{JI}) w z + n_{SP,p} \tag{4}$$

where  $n_{SU,k} \sim \mathcal{CN}(0, \delta^2)$ ,  $n_{SEVE,l} \sim \mathcal{CN}(0, \delta^2)$ ,  $n_{SEH,j} \sim \mathcal{CN}(0, \delta^2)$ , and  $n_{SP,p} \sim \mathcal{CN}(0, \delta^2)$  are the additional noise. Henceforth, the SINR referred to the  $k$ -th cognitive IoT device is

$$\gamma_{SU,k} = \frac{|(h_{BU,k}^H + h_{IU,k}^H \Theta H_{BI}) f_k|^2}{\sum_{i=1, i \neq k}^K |(h_{BU,k}^H + h_{IU,k}^H \Theta H_{BI}) f_i|^2 + |(g_{JU,k}^H + g_{IU,k}^H \Theta G_{JI}) w|^2 + \delta^2} \tag{5}$$

The SINR referred to the  $l$ -th eavesdropper can be formulated as

$$\gamma_{SE,l} = \frac{|(h_{BEVE,l}^H + h_{IEVE,l}^H \Theta H_{BI}) f_k|^2}{\sum_{i=1, i \neq k}^K |(h_{BEVE,l}^H + h_{IEVE,l}^H \Theta H_{BI}) f_i|^2 + |(g_{JEVE,l}^H + g_{IEVE,l}^H \Theta G_{JI}) w|^2 + \delta^2} \tag{6}$$

As a result, the achievable secure rate of  $k$ -th IoT device is

$$R_{s,k} = \max \left[ \log_2(1 + \gamma_{SU,k}) - \max_{\forall l} \log_2(1 + \gamma_{SE,l}), 0 \right] \tag{7}$$

In CR networks, PUs enjoy higher priority in terms of spectrum utilization than SUs. As SUs communicate through a shared spectrum, they may potentially interfere with PUs. To safeguard the performance of  $p$ -th PUs, the interference power experienced by the PUs is effectively constrained to remain beneath a predefined threshold, which is denoted by:

$$\sum_{i=1}^K |(h_{BP,p}^H + h_{IP,p}^H \Theta H_{BI}) f_i|^2 + |(g_{JP,p}^H + g_{IP,p}^H \Theta G_{JI}) w|^2 + \delta^2 \leq \Gamma_0 \tag{8}$$

where  $\Gamma_0$  is the interference threshold. Additionally, the collected power of the  $j$ -th EHR is modeled as

$$E_j = \sum_{i=1}^K |(\mathbf{h}_{BEH,j}^H + \mathbf{h}_{IEH,j}^H \Theta \mathbf{H}_{BI}) \mathbf{f}_i|^2 + |(\mathbf{g}_{JEH,j}^H + \mathbf{g}_{IEH,j}^H \Theta \mathbf{G}_{JI}) \mathbf{w}|^2 \quad (9)$$

Since the received signal power is considerably higher than the noise power, the energy harvesting module needs to be activated by the relatively high energy carried by the received radio frequency (RF) signal (about  $-10$  dBm). If the received RF signal energy is lower than the minimum threshold, energy cannot be harvested. Therefore, this article disregards the energy harvested from noise power.

### 3. Secure Transmission Algorithm Design

#### 3.1. Problem Formulation

Drawing on the aforementioned analysis, this study endeavors to maximize the sum harvested energy at the EHRs by means of a joint optimization approach, involving the SBS's beamforming vector, the jammer's interference precoding vector, and the IRS's phase-shift matrix. The optimization problem is subject to several constraints, including the SBS's total transmission power, the jammer's total power, the interference constraint at the PUs, the secure rate of each cognitive IoT device, and the phase shift is enforced to possess a unitary modulus. The considered problem can be mathematically modeled as:

$$\begin{aligned} \max_{\mathbf{f}_k, \mathbf{w}, \Theta} & \sum_{j=1}^J \sum_{i=1}^K |(\mathbf{h}_{BEH,j}^H + \mathbf{h}_{IEH,j}^H \Theta \mathbf{H}_{BI}) \mathbf{f}_i|^2 + \\ & \sum_{j=1}^J |(\mathbf{g}_{JEH,j}^H + \mathbf{g}_{IEH,j}^H \Theta \mathbf{G}_{JI}) \mathbf{w}|^2 \\ \text{s.t.} & \text{C1: } \sum_{i=1}^K \|\mathbf{f}_i\|^2 \leq P_s \\ & \text{C2: } \|\mathbf{w}\|^2 \leq P_j \\ & \text{C3: } R_{s,k} \geq R_{s,th}, \forall k \\ & \text{C4: } \sum_{i=1}^K |(\mathbf{h}_{BP,p}^H + \mathbf{h}_{IP,p}^H \Theta \mathbf{H}_{BI}) \mathbf{f}_i|^2 + \\ & |(\mathbf{g}_{JP,p}^H + \mathbf{g}_{IP,p}^H \Theta \mathbf{G}_{JI}) \mathbf{w}|^2 + \delta^2 \leq \Gamma_0 \\ & \text{C5: } 0 \leq \theta_n \leq \pi \forall n \end{aligned} \quad (10)$$

where  $R_{s,th}$  indicates the minimum secure rate threshold of the  $k$ -th IoT device, and  $P_s$  and  $P_j$  represent the maximum allowable transmit power of the SBS and the IJ, respectively.

The constraint C1 restricts the maximum transmission power of the SBS, while C2 imposes limits on the maximum transmission power of the jammer. C3 and C4 are constraints that respectively regulate the secure rate at each IoT device and the interference impact on PUs. Moreover, C5 indicates the limitation of the phase shift of IRS. It is evident that the optimization problem presented in Equation (10) belongs to a non-convex as well as a multi-variable coupled problem that is challenging to solve directly due to the impact of the objective function and constraint C3. Consequently, obtaining optimal solutions for the SBS's beamforming vector, the IJ's interference precoding vector, and the phase-shift matrix requires a non-trivial approach. Hence, the following section aims to propose an iterative algorithm utilizing block coordinate descent to address the resource allocation problem with the goal of maximizing the total harvested energy.

In order to streamline the analysis of problem (10), we set

$$\begin{aligned}
 \mathbf{u} &= [e^{j\theta_1}, \dots, e^{j\theta_N}], \mathbf{v} = [\mathbf{u}^H; 1], \\
 \mathbf{H}_{SU,k} &= [\text{diag}(\mathbf{h}_{IU,k}^H) \mathbf{H}_{BI}; \mathbf{h}_{BU,k}^H] \\
 \mathbf{H}_{SEVE,i} &= [\text{diag}(\mathbf{h}_{IEVE,i}^H) \mathbf{H}_{BI}; \mathbf{h}_{BEVE,i}^H] \\
 \mathbf{H}_{SEH,j} &= [\text{diag}(\mathbf{h}_{IEH,j}^H) \mathbf{H}_{BI}; \mathbf{h}_{BEH,j}^H] \\
 \mathbf{H}_{SP,p} &= [\text{diag}(\mathbf{h}_{IP,p}^H) \mathbf{H}_{BI}; \mathbf{h}_{BP,p}^H] \\
 \mathbf{G}_{JU,k} &= [\text{diag}(\mathbf{g}_{IU,k}^H) \mathbf{G}_{JI}; \mathbf{g}_{JU,k}^H] \\
 \mathbf{G}_{JEVE,i} &= [\text{diag}(\mathbf{g}_{IEVE,i}^H) \mathbf{G}_{JI}; \mathbf{g}_{JEVE,i}^H] \\
 \mathbf{G}_{JEH,j} &= [\text{diag}(\mathbf{g}_{IEH,j}^H) \mathbf{G}_{JI}; \mathbf{g}_{JEH,j}^H] \\
 \mathbf{G}_{JP,p} &= [\text{diag}(\mathbf{g}_{IP,p}^H) \mathbf{G}_{JI}; \mathbf{g}_{JP,p}^H]
 \end{aligned} \tag{11}$$

Hence , problem (10) can reformulated as

$$\begin{aligned}
 \max_{\mathbf{f}_k, \mathbf{w}, \mathbf{v}} & \sum_{j=1}^J \left( \sum_{i=1}^K |\mathbf{v}^H \mathbf{H}_{SEH,j} \mathbf{f}_i|^2 + |\mathbf{v}^H \mathbf{G}_{JEH,j} \mathbf{w}|^2 \right) \\
 \text{s.t. C1:} & \sum_{i=1}^K \|\mathbf{f}_i\|^2 \leq P_s \\
 \text{C2:} & \|\mathbf{w}\|^2 \leq P_j \\
 \text{C3:} & \log_2(1 + \tilde{\gamma}_{SU,k}) - \max_{\forall l} \log_2(1 + \tilde{\gamma}_{SE,l}) \geq R_{s,th}, \forall k \\
 \text{C4:} & \sum_{i=1}^K |\mathbf{v}^H \mathbf{H}_{SP,p} \mathbf{f}_i|^2 + |\mathbf{v}^H \mathbf{G}_{JP,p} \mathbf{w}|^2 + \delta^2 \leq \Gamma_0 \\
 \text{C5:} & |\mathbf{v}(1, n)| = 1
 \end{aligned} \tag{12}$$

where

$$\tilde{\gamma}_{SU,k} = \frac{|\mathbf{v}^H \mathbf{H}_{SU,k} \mathbf{f}_k|^2}{\sum_{i=1, i \neq k}^K |\mathbf{v}^H \mathbf{H}_{SU,k} \mathbf{f}_i|^2 + |\mathbf{v}^H \mathbf{G}_{JU,k} \mathbf{w}|^2 + \delta^2} \tag{13}$$

$$\tilde{\gamma}_{SE,l} = \frac{|\mathbf{v}^H \mathbf{H}_{SEVE,l} \mathbf{f}_k|^2}{\sum_{i=1, i \neq k}^K |\mathbf{v}^H \mathbf{H}_{SEVE,l} \mathbf{f}_i|^2 + |\mathbf{v}^H \mathbf{G}_{JEVE,l} \mathbf{w}|^2 + \delta^2} \tag{14}$$

Since the secrecy rate constraint expressed in  $\bar{\text{C3}}$  is non-convex, it can be approximated using convex techniques, such as introducing slack variables and utilizing SPCA techniques. To facilitate the handling of Constraint ( $\bar{\text{C3}}$ ), two slack variables,  $t_{1,k}$  and  $t_{2,k}$ , are introduced, which results in an equivalent transformation of the original Equation ( $\bar{\text{C3}}$ ) for easier processing, such as

$$\begin{aligned}
 \log_2(t_{1,k} t_{2,k}) & \geq R_{s,th} \\
 1 + \frac{|\mathbf{v}^H \mathbf{H}_{SU,k} \mathbf{f}_k|^2}{\sum_{i=1, i \neq k}^K |\mathbf{v}^H \mathbf{H}_{SU,k} \mathbf{f}_i|^2 + |\mathbf{v}^H \mathbf{G}_{JU,k} \mathbf{w}|^2 + \delta^2} & \geq t_{1,k} \\
 1 + \frac{|\mathbf{v}^H \mathbf{H}_{SEVE,l} \mathbf{f}_k|^2}{\sum_{i=1, i \neq k}^K |\mathbf{v}^H \mathbf{H}_{SEVE,l} \mathbf{f}_i|^2 + |\mathbf{v}^H \mathbf{G}_{JEVE,l} \mathbf{w}|^2 + \delta^2} & \leq \frac{1}{t_{2,k}}
 \end{aligned} \tag{15}$$

Furthermore , expression ( $\bar{\text{C3}}$ ) can undergo a conversion to

$$\begin{aligned}
 \bar{C}3 - 1 : t_{1,k}t_{2,k} &\geq 2^{R_{s,th}} \\
 \bar{C}3 - 2 : \frac{|v^H H_{SU,k} f_k|^2}{\sum_{i=1, i \neq k}^K |v^H H_{SU,k} f_i|^2 + |v^H G_{JU,k} w|^2 + \delta^2} &\geq t_{1,k} - 1 \\
 \bar{C}3 - 3 : \frac{\sum_{i=1, i \neq k}^K |v^H H_{SEVE,l} f_i|^2 + |v^H G_{JEVE,l} w|^2 + \delta^2}{\sum_{i=1}^K |v^H H_{SEVE,l} f_i|^2 + |v^H G_{JEVE,l} w|^2 + \delta^2} &\geq t_{2,k}
 \end{aligned} \tag{16}$$

The constraint condition expressed in Equation (12) is equivalent to

$$2^{R_{s,th}+2} + (t_{1,k} - t_{2,k})^2 \leq (t_{1,k} + t_{2,k})^2 \tag{17}$$

In addition, (16) can be reformulated into a quadratic function representation, thereby yielding

$$\|[\sqrt{2^{R_{s,th}+2}}, t_{1,k} - t_{2,k}]\| \leq t_{1,k} + t_{2,k} \tag{18}$$

Consequently, we can rephrase problem (12) as

$$\begin{aligned}
 \max_{t_{1,k}, t_{2,k}, f_k, w, v} & \sum_{j=1}^J \left( \sum_{i=1}^K |v^H H_{SEH,j} f_i|^2 + |v^H G_{JEH,j} w|^2 \right) \\
 s.t. & C1, \bar{C}3 - 2, \bar{C}3 - 3, \bar{C}4, C5 \\
 & \|[\sqrt{2^{R_{s,th}+2}}, t_{1,k} - t_{2,k}]\| \leq t_{1,k} + t_{2,k}, \forall k
 \end{aligned} \tag{19}$$

In comparison to the pre-transformation problem (12), the post-transformation problem (19) exhibits a higher tractability for the solution. However, due to the convex nature of the cost function, the presence of non-convex constraints denoted as  $\bar{C}3 - 2$  and  $\bar{C}3 - 3$ , as well as the interconnectedness among variables  $t_{1,k}, t_{2,k}, f_k, w, v, \forall k$ , the attainment of the optimal solutions for variables  $t_{1,k}, t_{2,k}, f_k, w, v, \forall k$  remains elusive using conventional convex optimization theories. Hence, the subsequent section will introduce a novel approach, utilizing an iterative algorithm that employs a block coordinate descent (BCD) approach to address the non-convex resource allocation problem that aims to maximize both collection and energy.

### 3.2. Proposed Algorithm

In this section, we delve into the application of the BCD method as a means to untangle the intricacies of problem (19), effectively segregating it into two discernible subproblems. More precisely, our initial focus revolves around the subproblem of devising an optimal transmit beamforming scheme for both the SBS and cognitive jammer, while duly taking into account the existence of a given phase-shift matrix that governs the behavior of IRS. To tackle this subproblem, we employ a refined continuous convex approximation technique, tailored to ensure a reliable and accurate solution. Subsequently, leveraging the acquired transmit beamforming shaping vector for the cognitive base station in tandem with the transmit beamforming vector for the cognitive jammer, we proceed to employ the widely embraced SDR methodology.

#### 3.2.1. Cognitive Beamforming Vector Optimization

In the presence of a pre-determined phase-shift matrix  $\text{diag}(v)$ , we encounter an optimization quandary concerning the strategic formulation of the transmit beamforming shaping vector for the SBS, as well as the interference beamforming vector for the jammer. This optimization predicament can be succinctly expounded upon in the subsequent manner:

$$\begin{aligned}
 & \max_{f_k, \mathbf{w}, t_{1,k}, t_{2,k}} \sum_{j=1}^J \left( \sum_{i=1}^K |v^H \mathbf{H}_{SEH,j} f_i|^2 + |v^H \mathbf{G}_{JEH,j} \mathbf{w}|^2 \right) \\
 & \text{s.t. } C1, C2, \bar{C}4 \\
 & \bar{C}3 - 1 : \|\sqrt{2^{R_{s,th}+2}}, t_{1,k} - t_{2,k}\| \leq t_{1,k} + t_{2,k}, \forall k \\
 & \bar{C}3 - 2 : \frac{|v^H \mathbf{H}_{SU,k} f_k|^2}{\sum_{i=1, i \neq k}^K |v^H \mathbf{H}_{SU,k} f_i|^2 + |v^H \mathbf{G}_{JU,k} \mathbf{w}|^2 + \delta^2} \geq t_{1,k} - 1 \\
 & \bar{C}3 - 3 : \frac{\sum_{i=1, i \neq k}^K |v^H \mathbf{H}_{SEVE,l} f_i|^2 + |v^H \mathbf{G}_{JEVE,l} \mathbf{w}|^2 + \delta^2}{\sum_{i=1}^K |v^H \mathbf{H}_{SEVE,l} f_i|^2 + |v^H \mathbf{G}_{JEVE,l} \mathbf{w}|^2 + \delta^2} \geq t_{2,k}
 \end{aligned} \tag{20}$$

Owing to the intricate interplay between the objective function and non-convex constraints  $\bar{C}3 - 2$  and  $\bar{C}3 - 3$ , problem (20) remains inherently non-convex in nature. Moreover, it is of significance to observe that the constraints  $\bar{C}3 - 2$  and  $\bar{C}3 - 3$  can be elegantly reformulated as follows:

$$\begin{aligned}
 & \sum_{i=1, i \neq k}^K |v^H \mathbf{H}_{SU,k} f_i|^2 + |v^H \mathbf{G}_{JU,k} \mathbf{w}|^2 \leq \frac{|v^H \mathbf{H}_{SU,k} f_k|^2}{t_{1,k} - 1} - \delta^2 \\
 & \frac{\sum_{i=1, i \neq k}^K |v^H \mathbf{H}_{SEVE,l} f_i|^2 + |v^H \mathbf{G}_{JEVE,l} \mathbf{w}|^2 + \delta^2}{t_{2,k}} \geq \\
 & \sum_{i=1}^K |v^H \mathbf{H}_{SEVE,l} f_i|^2 + |v^H \mathbf{G}_{JEVE,l} \mathbf{w}|^2 + \delta^2
 \end{aligned} \tag{21}$$

Notwithstanding its non-convex nature and the inherent challenges associated with obtaining solutions, we address this predicament via the utilization of the SCA technique, which enable the transformation of the problem at hand. Specifically, when considering a differentiable convex function  $g(x)$ , it becomes feasible to approximate it utilizing a tangential function denoted as  $f(x, \bar{x})$ . This tangential function represents the first-order Taylor expansion centered around the point  $\bar{x}$  [33]. Consequently, we can express the resultant relationship as follows:

$$g(x) \geq f(x, \bar{x}) = g(\bar{x}) + \nabla_x g(\bar{x})(x - \bar{x}) \tag{22}$$

The above equation holds true when  $x$  is equal to  $\bar{x}$ . Building upon the preceding Taylor series approximation, Lemma 1 is introduced as a viable approximation technique for Equation (21).

**Lemma 1.** *Two functions is modeled as*

$$\begin{aligned}
 Q_1(t_{1,k}, f_k) &= \frac{|v^H \mathbf{H}_{SU,k} f_k|^2}{t_{1,k} - 1} - \delta^2 \\
 Q_2(t_{2,k}, \mathbf{w}, f_k) &= \frac{\sum_{i=1, i \neq k}^K |v^H \mathbf{H}_{SEVE,l} f_i|^2 + |v^H \mathbf{G}_{JEVE,l} \mathbf{w}|^2 + \delta^2}{t_{2,k}}
 \end{aligned} \tag{23}$$

Then, a first-order Taylor approximation of  $Q_1(t_{1,k}, f_k)$  and  $Q_2(t_{2,k}, \mathbf{w}, f_k)$  centered around the reference point  $(\bar{t}_{1,k}, \bar{t}_{2,k}, \bar{\mathbf{w}}, \bar{f}_k)$  can be formulated as

$$Q_3(t_{1,k}, f_k, \bar{t}_{1,k}, \bar{w}, \bar{f}_k) = \frac{2\text{Re}\{ \bar{f}_k^H \mathbf{H}_{SU,k}^H \mathbf{v} \mathbf{v}^H \mathbf{H}_{SU,k} \bar{f}_k \}}{\bar{t}_{1,k} - 1} - \delta^2 - \frac{\text{Re}\{ \bar{f}_k^H \mathbf{H}_{SU,k}^H \mathbf{v} \mathbf{v}^H \mathbf{H}_{SU,k} \bar{f}_k \}}{(\bar{t}_{1,k} - 1)^2} (t_{1,k} - 1) \tag{24}$$

$$Q_4(t_{2,k}, w, f_k, \bar{t}_{2,k}, \bar{w}, \bar{f}_k) = \frac{\sum_{i=1, i \neq k}^K 2\text{Re}(v^H \mathbf{H}_{SEVE,l} f_i \bar{f}_i^H \mathbf{H}_{SEVE,l}^H v)}{\bar{t}_{2,k}} + \frac{2\text{Re}(v^H \mathbf{G}_{JEVE,l} w \bar{w}^H \mathbf{G}_{JEVE,l} w^H v)}{\bar{t}_{2,k}} + \frac{\delta^2}{\bar{t}_{2,k}^2} (2\bar{t}_{2,k} - t_{2,k}) - \frac{\sum_{i=1, i \neq k}^K 2\text{Re}(v^H \mathbf{H}_{SEVE,l} \bar{f}_i \bar{f}_i^H \mathbf{H}_{SEVE,l}^H v)}{\bar{t}_{2,k}^2} - \frac{2\text{Re}(v^H \mathbf{G}_{JEVE,l} \bar{w} \bar{w}^H \mathbf{G}_{JEVE,l} w^H v)}{\bar{t}_{2,k}^2} \tag{25}$$

By adopting these approaches, we can effectively substitute  $Q_1(t_{1,k}, w, f_k)$  and  $Q_2(t_{2,k}, w, f_k)$  with  $Q_3(t_{1,k}, w, f_k, \bar{t}_{1,k}, \bar{w}, \bar{f}_k)$  and  $Q_4(t_{2,k}, w, f_k, \bar{t}_{2,k}, \bar{w}, \bar{f}_k)$ , respectively, leading to a streamlined formulation.

**Proof.** Utilizing the Taylor series approximation as stated in Equations (24) and (25), we derive

$$Q_1(t_{1,k}, f_k) \geq Q_3(\bar{t}_{1,k}, \bar{f}_k) + \left. \frac{\partial Q_3}{\partial f_k} \right|_{(\bar{t}_{1,k}, \bar{f}_k)} (f_k - \bar{f}_k) + \left. \frac{\partial Q_3}{\partial t_{1,k}} \right|_{(\bar{t}_{1,k}, \bar{f}_k)} (t_{1,k} - \bar{t}_{1,k}) - \delta^2 = Q_3(t_{1,k}, f_k, \bar{t}_{1,k}, \bar{w}, \bar{f}_k) \tag{26}$$

$$Q_2(t_{2,k}, w, f_k) \geq Q_4(\bar{t}_{1,k}, \bar{f}_k, \bar{w}) + \left. \frac{\partial Q_4}{\partial f_k} \right|_{(\bar{t}_{1,k}, \bar{f}_k)} (f_k - \bar{f}_k) + \left. \frac{\partial Q_4}{\partial t_{1,k}} \right|_{(\bar{t}_{1,k}, \bar{f}_k)} (t_{1,k} - \bar{t}_{1,k}) - \delta^2 = Q_4(t_{1,k}, f_k, \bar{t}_{1,k}, \bar{w}, \bar{f}_k) \tag{27}$$

where

$$Q_3(t_{1,k}, f_k, \bar{t}_{1,k}, \bar{w}, \bar{f}_k) = \frac{v^H \mathbf{H}_{SU,k} \bar{f}_k \bar{f}_k^H \mathbf{H}_{SU,k}^H v}{\bar{t}_{1,k} - 1} - \delta^2 + \frac{2\bar{f}_k^H \mathbf{H}_{SU,k}^H v \mathbf{v}^H \mathbf{H}_{SU,k} \bar{f}_k}{\bar{t}_{1,k} - 1} (f_k - \bar{f}_k) - \frac{v^H \mathbf{H}_{SU,k} \bar{f}_k \bar{f}_k^H \mathbf{H}_{SU,k}^H v}{(\bar{t}_{1,k} - 1)^2} [(t_{1,k} - 1) - (\bar{t}_{1,k} - 1)] \tag{28}$$

$$\begin{aligned}
 Q_4(t_{1,k}, f_k, \bar{t}_{1,k}, \bar{w}, \bar{f}_k) &= \frac{\sum_{i=1, i \neq k}^K v^H \mathbf{H}_{SEVE,l} \bar{f}_i \bar{f}_i^H \mathbf{H}_{SEVE,l}^H v}{\bar{t}_{2,k}} + \\
 &+ \frac{\sum_{i=1, i \neq k}^K 2\bar{f}_i^H \mathbf{H}_{SEVE,l}^H v v^H \mathbf{H}_{SEVE,l}}{\bar{t}_{2,k}} (f_i - \bar{f}_i) \\
 &+ \frac{2\bar{w}^H \mathbf{G}_{JEVE,l}^H v v^H \mathbf{G}_{JEVE,l}}{\bar{t}_{2,k}} (w - \bar{w}) + \frac{v^H \mathbf{G}_{JEVE,l} \bar{w} \bar{w}^H \mathbf{G}_{JEVE,l}^H v}{\bar{t}_{2,k}} \\
 &- \frac{\sum_{i=1, i \neq k}^K |v^H \mathbf{H}_{SEVE,l} \bar{f}_i|^2 + |v^H \mathbf{G}_{JEVE,l} \bar{w}|^2}{\bar{t}_{2,k}^2} (t_{2,k} - \bar{t}_{2,k})
 \end{aligned} \tag{29}$$

To better approximate the real nature of the functions  $Q_1(t_{1,k}, f_k)$  and  $Q_2(t_{2,k}, w, f_k)$ , Equations (28) and (29) can be further modified as

$$\begin{aligned}
 Q_3(t_{1,k}, f_k, \bar{t}_{1,k}, \bar{w}, \bar{f}_k) &= \frac{2\text{Re}\{v^H \mathbf{H}_{SU,k} \bar{f}_k \bar{f}_k^H \mathbf{H}_{SU,k}^H v\}}{\bar{t}_{1,k} - 1} - \delta^2 \\
 &- \frac{\text{Re}\{v^H \mathbf{H}_{SU,k} \bar{f}_k \bar{f}_k^H \mathbf{H}_{SU,k}^H v\}}{(\bar{t}_{1,k} - 1)^2} (t_{1,k} - 1) \\
 &= \frac{2\text{Re}\{\bar{f}_k^H \mathbf{H}_{SU,k}^H v v^H \mathbf{H}_{SU,k} \bar{f}_k\}}{\bar{t}_{1,k} - 1} - \delta^2 \\
 &- \frac{\text{Re}\{\bar{f}_k^H \mathbf{H}_{SU,k}^H v v^H \mathbf{H}_{SU,k} \bar{f}_k\}}{(\bar{t}_{1,k} - 1)^2} (t_{1,k} - 1)
 \end{aligned} \tag{30}$$

$$\begin{aligned}
 Q_4(t_{1,k}, f_k, \bar{t}_{1,k}, \bar{w}, \bar{f}_k) &= \frac{\sum_{i=1, i \neq k}^K 2\text{Re}(v^H \mathbf{H}_{SEVE,l} \bar{f}_i \bar{f}_i^H \mathbf{H}_{SEVE,l}^H v)}{\bar{t}_{2,k}} \\
 &+ \frac{2\text{Re}(v^H \mathbf{G}_{JEVE,l} \bar{w} \bar{w}^H \mathbf{G}_{JEVE,l} v)}{\bar{t}_{2,k}} + \frac{\delta^2}{\bar{t}_{2,k}^2} (2\bar{t}_{2,k} - t_{2,k}) \\
 &- \frac{\sum_{i=1, i \neq k}^K 2\text{Re}(v^H \mathbf{H}_{SEVE,l} \bar{f}_i \bar{f}_i^H \mathbf{H}_{SEVE,l}^H v)}{\bar{t}_{2,k}^2} \\
 &- \frac{2\text{Re}(v^H \mathbf{G}_{JEVE,l} \bar{w} \bar{w}^H \mathbf{G}_{JEVE,l} v)}{\bar{t}_{2,k}^2} \\
 &= \frac{\sum_{i=1, i \neq k}^K 2\text{Re}(\bar{f}_i^H \mathbf{H}_{SEVE,l}^H v v^H \mathbf{H}_{SEVE,l} \bar{f}_i)}{\bar{t}_{2,k}} \\
 &+ \frac{2\text{Re}(\bar{w}^H \mathbf{G}_{JEVE,l} v v^H \mathbf{G}_{JEVE,l} \bar{w})}{\bar{t}_{2,k}} + \frac{\delta^2}{\bar{t}_{2,k}^2} (2\bar{t}_{2,k} - t_{2,k}) \\
 &- \frac{\sum_{i=1, i \neq k}^K 2\text{Re}(\bar{f}_i^H \mathbf{H}_{SEVE,l}^H v v^H \mathbf{H}_{SEVE,l} \bar{f}_i)}{\bar{t}_{2,k}^2} \\
 &- \frac{2\text{Re}(\bar{w}^H \mathbf{G}_{JEVE,l} v v^H \mathbf{G}_{JEVE,l} \bar{w})}{\bar{t}_{2,k}^2}
 \end{aligned} \tag{31}$$

The validity of the approximations given in Equations (26) and (27) hinge on the fulfillment of the conditions  $f_i = \bar{f}_i$ ,  $w = \bar{w}$ ,  $t_{1,k} = \bar{t}_{1,k}$  and  $t_{2,k} = \bar{t}_{2,k}$ .

Based on the preceding derivation, we can approximate  $Q_1(t_{1,k}, f_k)$  and  $Q_2(t_{2,k}, w, f_k)$  as  $Q_3(t_{1,k}, f_k, \bar{t}_{1,k}, \bar{w}, \bar{f}_k)$  and  $Q_4(t_{2,k}, w, f_k, \bar{t}_{2,k}, \bar{w}, \bar{f}_k)$ , resulting in the transformation of Equation (23) into a convex form represented by Equations (24) and (25).  $\square$

However, (20) remains non-convex, primarily because of the objective function. Keep in mind that the quadratic nature of the objective function, involving  $w$  and  $f_i$ , can be addressed via the application of the following lemma to linearize them.

**Lemma 2.** *The following function is characterized as*

$$F_1(f_i, w) = \sum_{j=1}^J \left( \sum_{i=1}^K |v^H \mathbf{H}_{SEH,j} f_i|^2 + |v^H \mathbf{G}_{JEH,j} w|^2 \right) \quad (32)$$

The primary-order Taylor approximation of the function  $F_1(f_i, w)$  at a tangency point  $\bar{f}_i$  and  $\bar{w}$  can be articulated as

$$\begin{aligned} F_2(f_i, w, \bar{f}_i, \bar{w}) = & \sum_{j=1}^J \left( \sum_{i=1}^K 2\text{Re}(\bar{f}_i^H \mathbf{H}_{SEH,j}^H v v^H \mathbf{H}_{SEH,j} f_i) \right. \\ & - \text{Re}(\bar{f}_i^H \mathbf{H}_{SEH,j}^H v v^H \mathbf{H}_{SEH,j} \bar{f}_i) \\ & + 2\text{Re}(\bar{w}^H \mathbf{H}_{SEH,j}^H v v^H \mathbf{H}_{SEH,j} w) \\ & \left. - \text{Re}(\bar{w}^H \mathbf{H}_{SEH,j}^H v v^H \mathbf{H}_{SEH,j} \bar{w}) \right) \end{aligned} \quad (33)$$

Adopting this methodology permits the substitution of Equation (32) with Equation (33), thereby enabling the approximation of the objective function in (20) as a concave function.

**Proof.** Utilizing the Taylor series approximation, (32) exhibits differentiability and adheres to the following criteria:

$$F_1(f_i, w) \geq F_1(\bar{f}_i, \bar{w}) + \nabla F_1(\bar{f}_i, \bar{w})^H (f_i - \bar{f}_i) + \nabla F_1(\bar{f}_i, \bar{w})^H (w - \bar{w}) \quad (34)$$

Through the application of the derivative rule, the substitution of (32) into inequality (34) yields the following result:

$$\begin{aligned} F_1(f_i, w) \geq & \sum_{j=1}^J \left( \sum_{i=1}^K (v^H \mathbf{H}_{SEH,j} \bar{f}_i \bar{f}_i^H \mathbf{H}_{SEH,j}^H v \right. \\ & + 2v^H \mathbf{H}_{SEH,j} \bar{f}_i \mathbf{H}_{SEH,j}^H v (f_i - \bar{f}_i) \\ & + v^H \mathbf{H}_{SEH,j} \bar{w} \bar{w}^H \mathbf{H}_{SEH,j}^H v \\ & \left. + 2v^H \mathbf{H}_{SEH,j} \bar{w} \mathbf{H}_{SEH,j}^H v (w - \bar{w}) \right) \end{aligned} \quad (35)$$

when  $\bar{w} \bar{w}^H \succeq \mathbf{0}$  and  $v^H \mathbf{H}_{SEH,j} \mathbf{H}_{SEH,j}^H v \succeq \mathbf{0}$ , then we have

$$F_1(f_i, w) \triangleq F_2(f_i, w, \bar{f}_i, \bar{w}) \quad (36)$$

Based on the derivation presented above, we can approximate  $F_1(f_i, w)$  as  $F_2(f_i, w, \bar{f}_i, \bar{w})$ . □

Utilizing the aforementioned transformations, we can redefine Equation (20) into a tractable convex form. Additionally, for the purpose of minimizing computational complexity, we rephrase problem (20) as a second-order cone programming (SOCP) problem [33,34], as detailed in Equation (37), and this can be efficiently solved using CVX.

$$\begin{aligned}
 & \max_{f_i, \mathbf{w}, t_{1,k}, t_{2,k}} F_2(f_i, \mathbf{w}, \bar{f}_i, \bar{\mathbf{w}}) \\
 & \text{s.t.} \quad \|[f_1^H, \dots, f_k^H]^H\| \leq \sqrt{P_s} \\
 & \quad \|\mathbf{w}\| \leq \sqrt{P_J} \\
 & \quad \|[v^H \mathbf{H}_{SP,p} f_1; \dots; v^H \mathbf{H}_{SP,p} f_k; \delta]\| \leq \sqrt{\Gamma_0} \\
 & \quad \|\sqrt{2^{R_s, h+2}}, t_{1,k} - t_{2,k}\| \leq t_{1,k} + t_{2,k}, \forall k \\
 & \quad \|[2v^H \mathbf{H}_{SU,k} f_1, \dots, 2v^H \mathbf{H}_{SU,k} f_{k-1}, 2v^H \mathbf{H}_{SU,k} f_{k+1}, \\
 & \quad 2v^H \mathbf{H}_{SU,k} f_k, 2v^H \mathbf{G}_{JU,k} \mathbf{w}, Q_3(t_{1,k}, f_k, \bar{t}_{1,k}, \bar{\mathbf{w}}, \bar{f}_k) - 1]\| \leq \\
 & \quad Q_3(t_{1,k}, f_k, \bar{t}_{1,k}, \bar{\mathbf{w}}, \bar{f}_k) + 1 \\
 & \quad \|[2v^H \mathbf{H}_{SEVE,l} f_1, \dots, 2v^H \mathbf{H}_{SEVE,l} f_k, 2v^H \mathbf{G}_{SEVE,l} \mathbf{w}, \\
 & \quad 2\delta, Q_4(t_{1,k}, f_k, \bar{t}_{1,k}, \bar{\mathbf{w}}, \bar{f}_k) - 1]\| \leq \\
 & \quad Q_4(t_{1,k}, f_k, \bar{t}_{1,k}, \bar{\mathbf{w}}, \bar{f}_k) + 1
 \end{aligned} \tag{37}$$

### 3.2.2. Passive Beamforming Design for IRS

In the presence of the given SBS's beamforming vectors and the IJ's beamforming vectors as well as  $t_{1,k}$  and  $t_{2,k}$ , we conduct optimization for the phase-shift matrix. Before optimizing the phase-shift matrix, we define  $\mathbf{V} = \mathbf{v}\mathbf{v}^H$ ,  $\mathbf{W} = \mathbf{w}\mathbf{w}^H$  and  $\mathbf{F}_i = \mathbf{f}_i \mathbf{f}_i^H$ . Then, problem (19) can be recasted as

$$\begin{aligned}
 & \max_{\mathbf{V}} \sum_{j=1}^J \left( \sum_{i=1}^K \text{Tr}(\mathbf{H}_{SEH,j} \mathbf{F}_i \mathbf{H}_{SEH,j}^H \mathbf{V}) + \text{Tr}(\mathbf{G}_{JEH,j} \mathbf{W} \mathbf{G}_{JEH,j}^H \mathbf{V}) \right) \\
 & \text{s.t.} \quad \sum_{i=1}^K \text{Tr}(\mathbf{H}_{SP,p} \mathbf{F}_i \mathbf{H}_{SP,p}^H \mathbf{V}) + \text{Tr}(\mathbf{G}_{JP,p} \mathbf{W} \mathbf{G}_{JP,p}^H \mathbf{V}) + \sigma^2 \leq \Gamma_0 \\
 & \quad \frac{\text{Tr}(\mathbf{H}_{SU,k} \mathbf{F}_k \mathbf{H}_{SU,k}^H \mathbf{V})}{t_{1,k} - 1} \geq \sum_{i=1, i \neq k}^K \text{Tr}(\mathbf{H}_{SU,k} \mathbf{F}_i \mathbf{H}_{SU,k}^H \mathbf{V}) + \\
 & \quad \quad \text{Tr}(\mathbf{G}_{JU,k} \mathbf{W} \mathbf{G}_{JU,k}^H \mathbf{V}) + \delta^2 \\
 & \quad \sum_{i=1, i \neq k}^K \text{Tr}(\mathbf{H}_{SEVE,l} \mathbf{F}_i \mathbf{H}_{SEVE,l}^H \mathbf{V}) + \text{Tr}(\mathbf{G}_{JEVE,l} \mathbf{W} \mathbf{G}_{JEVE,l}^H \mathbf{V}) + \delta^2 \geq \\
 & \quad t_{2,k} \left( \sum_{i=1}^K \text{Tr}(\mathbf{H}_{SEVE,l} \mathbf{F}_i \mathbf{H}_{SEVE,l}^H \mathbf{V}) + \text{Tr}(\mathbf{G}_{JEVE,l} \mathbf{W} \mathbf{G}_{JEVE,l}^H \mathbf{V}) + \delta^2 \right) \\
 & \quad \mathbf{V} \succeq \mathbf{0}, \text{Rank}(\mathbf{V}) = 1
 \end{aligned} \tag{38}$$

Owing to the presence of rank-one constraints, it is important to emphasize that (38) remains inherently non-convex in nature. Employing the SDR method, and deliberately relaxing the  $\text{Rank}(\mathbf{V}) = 1$  constraint, allows us to reformulate (38) into a more amenable problem, denoted as (39).

$$\begin{aligned}
 & \max_{\mathbf{V}} \sum_{j=1}^I \left( \sum_{i=1}^K \text{Tr}(\mathbf{H}_{SEH,j} \mathbf{F}_i \mathbf{H}_{SEH,j}^H \mathbf{V}) + \text{Tr}(\mathbf{G}_{JEH,j} \mathbf{W} \mathbf{G}_{JEH,j}^H \mathbf{V}) \right) \\
 \text{s.t. } & \sum_{i=1}^K \text{Tr}(\mathbf{H}_{SP,p} \mathbf{F}_i \mathbf{H}_{SP,p}^H \mathbf{V}) + \text{Tr}(\mathbf{G}_{JP,p} \mathbf{W} \mathbf{G}_{JP,p}^H \mathbf{V}) + \sigma^2 \leq \Gamma_0 \\
 & \frac{\text{Tr}(\mathbf{H}_{SU,k} \mathbf{F}_k \mathbf{H}_{SU,k}^H \mathbf{V})}{t_{1,k} - 1} \geq \sum_{i=1, i \neq k}^K \text{Tr}(\mathbf{H}_{SU,k} \mathbf{F}_i \mathbf{H}_{SU,k}^H \mathbf{V}) + \\
 & \qquad \qquad \qquad \text{Tr}(\mathbf{G}_{JU,k} \mathbf{W} \mathbf{G}_{JU,k}^H \mathbf{V}) + \delta^2 \\
 & \sum_{i=1, i \neq k}^K \text{Tr}(\mathbf{H}_{SEVE,l} \mathbf{F}_i \mathbf{H}_{SEVE,l}^H \mathbf{V}) + \text{Tr}(\mathbf{G}_{JEVE,l} \mathbf{W} \mathbf{G}_{JEVE,l}^H \mathbf{V}) + \delta^2 \geq \\
 & t_{2,k} \left( \sum_{i=1}^K \text{Tr}(\mathbf{H}_{SEVE,l} \mathbf{F}_i \mathbf{H}_{SEVE,l}^H \mathbf{V}) + \text{Tr}(\mathbf{G}_{JEVE,l} \mathbf{W} \mathbf{G}_{JEVE,l}^H \mathbf{V}) + \delta^2 \right)
 \end{aligned} \tag{39}$$

In accordance with the findings outlined in reference [28], it is established that (39) constitutes an SDP problem, amenable to resolution via an optimization solver such as CVX [22]. Nonetheless, it is crucial to underscore that, as a general rule, the relaxed problem (39) does not guarantee the attainment of a rank-1 solution, thus implicating that  $\text{Rank}(\mathbf{V}) \neq 1$ . The optimal cost function value of (39), in this context, serves solely as an upper bound for (38). Consequently, the process of constructing a rank-1 solution from the high-rank optimal solution of (39) necessitates supplementary procedural steps. To elucidate this procedure, it commences with an SVD of matrix  $\mathbf{V}$ , i.e.,  $\mathbf{V} = \mathbf{U} \mathbf{\Lambda} \mathbf{U}^H$  with the unitary matrix  $\mathbf{U} = [\mathbf{u}_1, \dots, \mathbf{u}_{N+1}]$  and the diagonal matrix  $\mathbf{\Lambda}$ . Subsequently, the suboptimal solution  $\mathbf{v}^* = \mathbf{U} \mathbf{\Lambda}^{\frac{1}{2}} \mathbf{r}$  for (38) is derived, with  $\mathbf{r} \in \mathcal{C}^{N+1}$  symbolizing a randomly generated vector based on  $\text{CN}(0, \mathbf{I}_{N+1})$ . Leveraging independently generated Gaussian vectors  $\mathbf{r}$ , the objective function of (39) is approximated by selecting the maximum value achieved for the most favorable  $\mathbf{v}$  among all  $\mathbf{v}$ . In the final analysis, the value of  $\mathbf{v}$  can be determined by the application of Equation (40).

$$\mathbf{v} = \mathbf{e}^{j \arg \left( \frac{v_n^*}{v_{N+1}^*} \right)}, \forall n = 1, \dots, N \tag{40}$$

### 3.3. Proposed Algorithm

Applying the concept of alternating iterative algorithms to address the original optimization problem, (19) reveals an interesting behavior: the power harvested by the EHR demonstrates a monotonically increasing trend throughout the iterative process. Nevertheless, owing to the constraints on transmission power, the proposed algorithm ultimately converges to a steady-state value. It is worth emphasizing that, given the non-convex nature of the original optimization problem (10), this algorithm cannot ensure the attainment of the global optimum. Instead, the presented alternating iterative approach incrementally approaches the optimal solution. To be more precise, we designate the solutions obtained after  $t$  iterations of the alternating iterative algorithm as  $\mathbf{V}(t)$ ,  $\tilde{\mathbf{f}}_i(t)$ ,  $\mathbf{w}(t)$ ,  $t_{1,k}(t)$ ,  $t_{2,k}(t)$ , and  $E(t) = \sum_{j=1}^J E_j(t)$ . A detailed outline of the alternating iterative algorithm's procedure is provided in Algorithm 1.

---

**Algorithm 1** Proposed Secure Transmission Algorithm.

---

- 1: **Initialization:**  $t = 0, \mathbf{V}(0), \bar{f}_i(0), \mathbf{w}(0), t_{1,k}(0), t_{2,k}(0)$  and  $E(0)$ ;
  - 2: **Repeat**
    - $t = t + 1$ ;
    - Employ the CVX solver to tackle the problem presented in (37), yielding the solutions  $f_i(t), \mathbf{w}(t), t_{1,k}(t)$  and  $t_{2,k}(t)$  while keeping the  $\mathbf{V}$  fixed;
    - Employ the CVX solver to tackle the problem presented in (40), yielding the solutions  $\mathbf{V}(t)$  and  $t_{2,k}(t)$  while keeping the  $f_i(t), \mathbf{w}(t), t_{1,k}(t)$  fixed;
  - 3: **Until**  $|E(t + 1) - E(t)| \leq 10^{-4}$ .
  - 4: **end**
- 

3.4. Complexity Analysis

The overall complexity of the alternative algorithm we propose is derived from two components: subproblem 1 and subproblem 2. In each iteration of the alternative algorithm, we independently solve problems (37) and (39). To elaborate, the complexity associated with subproblem 1, addressing the non-linear convex problem (37), is

$$C_1 = I_1 \cdot \mathcal{O}((M + (P + J + K + L)M + 3(P + J + K + L))^{3.5} \log(\frac{1}{\epsilon_1})) \tag{41}$$

where  $\epsilon_1$  represents the given solution accuracy,  $I_1$  is the number of iterations before convergence, and  $(M + (P + J + K + L)M + 3(P + J + K + L))$  denotes the number of variables [20,26,27]. The complexity of subproblem 2 solving the SDP problem (39) is

$$C_2 = I_2 \cdot \mathcal{O}((N + 1)^{3.5} \log(\frac{1}{\epsilon_2})) \tag{42}$$

where  $N + 1$  represents the dimension of the semi-definite cone and  $I_2$  denotes the number of iterations for subproblem 2 to converge. In summary, the combined complexity of the proposed alternative algorithm is

$$C_{\ni} = I_3(C_1 + C_2) \tag{43}$$

where  $I_3$  represents the overall number of iterations performed by the alternative algorithm.

**4. Simulation Results**

This section presents numerical simulations that demonstrate the benefits of incorporating IRS into cognitive SWIPT-IoT networks. To build on previous studies [21,29], we analyze an IRS-assisted cognitive SWIPT system with a secondary transmitter located at (40, 0, 20), a jammer positioned at (40, 0, 15), and an IRS positioned at (0, 0, 10). Moreover, we assume that  $K = 3$  IoT receivers,  $L = 2$  eavesdroppers,  $J = 3$  EHRs, and  $P = 3$  PUs are randomly distributed within a circular area with a radius of 2 m centered at (20, 100, 0), (15, 85, 0), (15, 80, 0), (20, -50, 0), respectively. Both secondary transmitter and jammer are equipped with a total of four antennas, allowing for the transmission of one data stream to each individual IoT user. Simultaneously, all users have one antenna. The model for the large-scale path loss from either the SBS to the IRS or the IRS to the users is represented as follows:

$$a(d) = T_0(d/d_0)^{-\alpha} \tag{44}$$

where  $T_0 = -30$  dB refers to the path loss (PL) with  $d_0 = 1$  m, where  $d$  indicates the distance between two nodes, and  $\alpha$  indicates the PL exponent. Assuming that the channels associated with IRS are all Rician channels, while the channels from the SBS and the IJ to all users are Rayleigh fading channels. Let us suppose that the PL factors from the SBS or jammer to the RIS, IoT users, PUs, eavesdroppers, and EHRs are  $\alpha_{BI} = \alpha_{JI} = 2.2, \alpha_{SU} = \alpha_{JU} = 3.6, \alpha_{SP} = \alpha_{JP} = 3.6, \alpha_{SE} = \alpha_{JE} = 3.6,$  and  $\alpha_{SEH} = \alpha_{JEH} = 3.6,$  respectively. Similarly, the path loss factors from the RIS to the IoT users, PUs, eavesdroppers, and EHRs are  $\alpha_{ISU} = 2.2, \alpha_{IP} = 2.4, \alpha_{IE} = 2.4$  and  $\alpha_{IEH} = 2.4,$  respectively. To evaluate the effectiveness of our

proposed algorithm, we have conducted a series of comparative analyses with other state-of-the-art algorithms. Specifically, we compared our algorithm with the following schemes: Baseline 1, which employs IRS for secure transmission without a jammer [34]; Baseline 2, which adopts reflective phase randomization with optimization based on Algorithm 1's active beamforming [30]; and Baseline 3, which is a secure transmission algorithm that does not rely on IRS assistance [29].

Figure 2 depicts the variation in the collected energy of EHRs over the iteration number with regard to the proposed secure signal scheme. The graph illustrates that the proposed algorithm achieves convergence after only a few iterations, indicating its superior convergence properties. Moreover, as the interference temperature experienced by the PU increases, the system's energy collection capability also grows. This phenomenon is due to the fact that, with a rise in the interference temperature, the PU can tolerate larger degrees of interference. Consequently, the constraints on the energy collection of secondary IoT users loosen, leading to an increase in the amount of energy they collect.

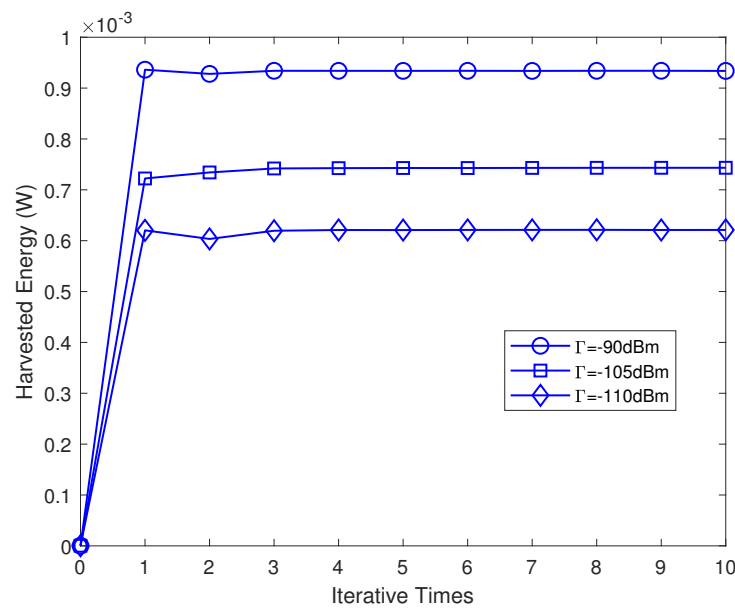


**Figure 2.** The collected energy varies with iteration number.

Figure 3 depicts the correlation between the energy harvested by EHR and the transmit power of the SBS employed for EHR collection. As indicated in Figure 3, the energy harvested by EHR for all four schemes consistently increases in a monotonic manner as the transmit power of the SBS augments, with the proposed scheme achieving the highest performance. The rationale behind this finding is as follows: in comparison to the scheme without IRS assistance, the inclusion of IRS can offer supplementary transmission paths for energy harvesting from the SBS to EHR. Further, when contrasted with the random phase scheme of IRS, optimizing the IRS phase results in an improved transmission of information to authorized users and energy users, rather than unauthorized users. Additionally, as  $P_s$  escalates, the performance gap between the IRS scheme and the non-IRS scheme, as well as the performance gap between the IRS phase optimization scheme and the random phase scheme, progressively intensifies. This is because the proposed scheme presented in this study reinforces the expected reflected signal directionally, which ultimately elevates the spatial degrees of freedom and diversity gain brought about by IRS.

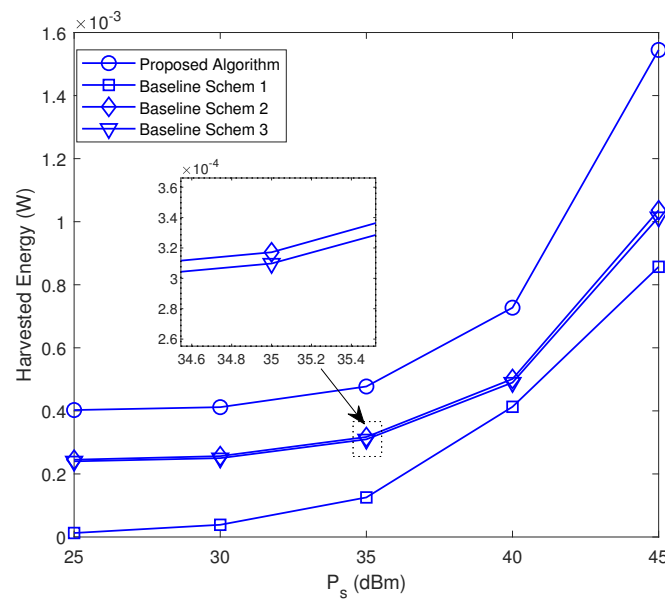


Figure 3. The correlation between the energy harvested by EHR and  $P_s$ .

Figure 4 depicts the correlation between the energy harvested by the EHRs and the transmit power of a jammer. The findings reveal that, except for the no-jammer scheme, the energy collected by the EHR increases as the transmit power rises for the other three schemes. Among the schemes with the same jammer power, the proposed scheme surpasses the scheme without IRS by approximately 1.84 dB. A comparative analysis indicates that the system assisted by IRS offers a more substantial enhancement in energy harvesting performance than the non-IRS scheme. Nonetheless, in the low power region, the scheme without the jammer exhibits superiority over the scheme without RIS and the random phase scheme. As the transmit power of the jammer increases, the performance gap between the proposed scheme and the other three comparative schemes widens. This outcome results from the fact that the proposed scheme can achieve a higher power degree of freedom through the jammer and effectively mitigate the eavesdropping rate of the eavesdropper. This approach broadens the feasible region of the security rate constraint and enhances the energy harvesting performance of the EHR.

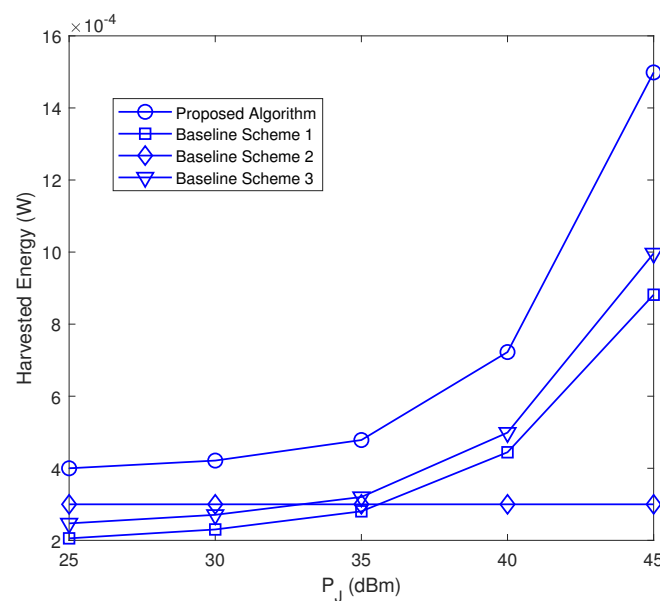
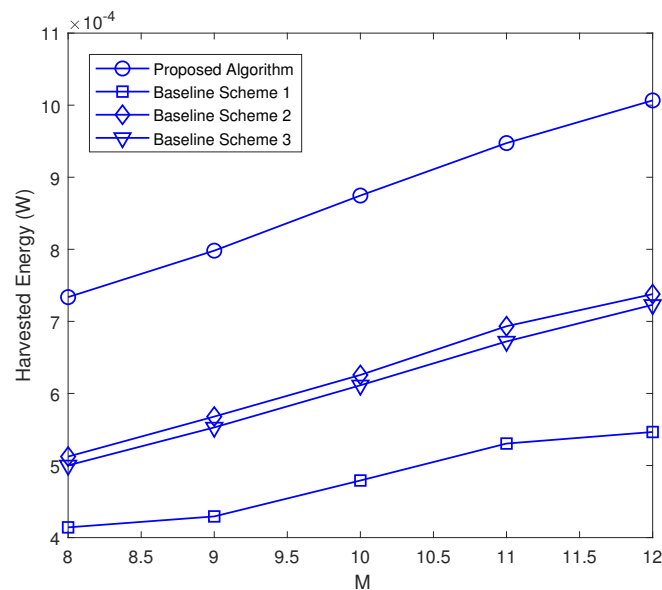


Figure 4. The correlation between the energy harvested by EHR and  $P_j$ .

The outcome depicted in Figure 5 demonstrates the correlation between the quantity of transmitting antennas, denoted as  $M$  for SBS, and the harvested energy levels, assessed across various benchmark schemes. It is evident that increasing the number of SBS's transmitting antennas leads to a significant improvement in the harvested energy in all evaluated scenarios. Specifically, augmenting the quantity of antennas can lead to greater energy beamforming gain and signal beamforming advantage, which enhances the beamforming effect and subsequently increases the energy harvested by the system. Therefore, utilizing multiple transmitting antennas in SBS can be an effective approach to improve the harvested energy of our considered communication systems. To provide further clarification, the proposed algorithm exhibits a substantial improvement of approximately  $3.2 \times 10^{-4}$  W in harvested energy as compared to the baseline scheme 1, which does not utilize IRS, when the number of transmitting antennas at the SBS is set to  $M = 8$ . Additionally, the algorithm achieves a noteworthy increment of around  $4.9 \times 10^{-4}$  W in harvested power at  $M = 12$ .



**Figure 5.** The correlation between the energy harvested by EHR and  $M$ .

Figure 6 depicts the curve that illustrates the relationship between the energy acquired by the EHR and the quantity of reflecting elements in the IRS represented as  $N$ . Assuming  $R_{s,th} = 3$  bps, the proposed methodology exhibits a monotonically increasing trend in the energy collected by the EHR as the number of IRS reflecting elements increases from 20 to 60. This phenomenon can be ascribed to the supplementary spatial DoF made available via the augmentation in the quantity of reflecting elements, which enhances the flexibility of passive beamforming and ameliorates the channel quality of the links between the SBS, IRS, and user devices, thereby elevating the overall energy harvesting performance of the CR system. When compared to three alternative algorithms, the proposed methodology outperforms them in terms of energy harvesting performance. Specifically, the IRS-assisted secure algorithm that is free from interference outshines the random phase optimization algorithm in terms of energy harvesting performance, thus emphasizing the paramount importance of phase optimization. As such, it is evident that the incorporation of IRS into SWIPT systems is a necessary undertaking.

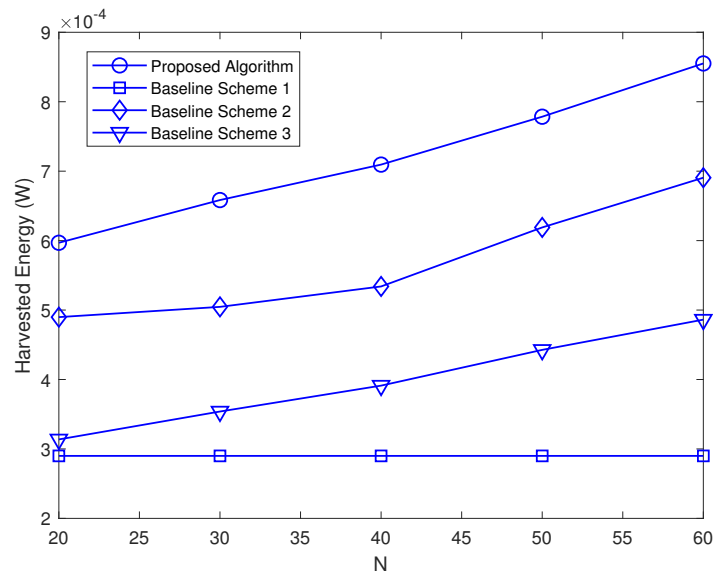


Figure 6. The correlation between the energy harvested by EHR and  $N$ .

Figure 7 illustrates the relationship between the energy harvested by the EHR and the secrecy rate. As shown in Figure 7, when  $M = 8$  and  $N = 50$ , the energy harvested by the EHR decreases gradually as the secrecy rate increases. Comparing the proposed energy harvesting scheme with three benchmark approaches, the energy harvesting performance of the system is found to be approximately 3.02 dB higher with IRS-assisted energy harvesting than that without IRS. This improvement can be attributed to the additional DoF and diversity gains provided by the IRS, as well as the optimization of IRS phase shifts that enhances the energy harvesting performance of the EHR. Notably, the proposed approach outperforms both the non-IRS and random phase shift approaches. Furthermore, compared to the non-jammer scheme, Figure 7 corroborates the efficacy of the proposed approach, which demonstrates a higher energy harvesting capability than the former at the same secrecy rate.

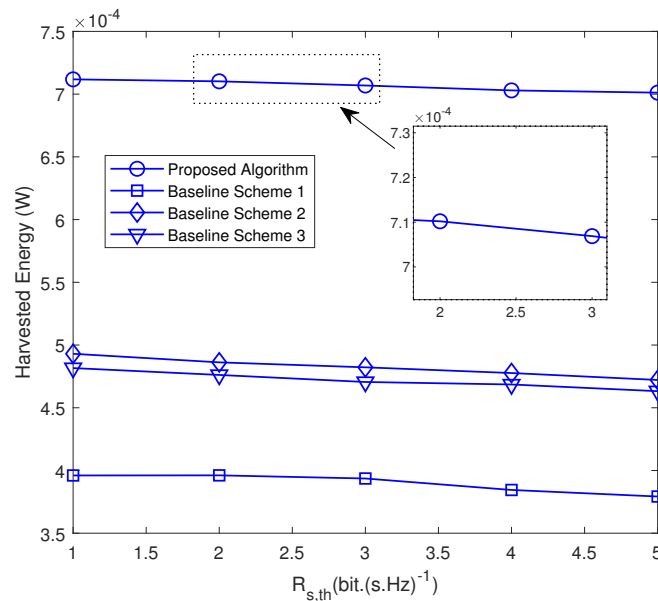


Figure 7. The correlation between the energy harvested by EHR and  $R_{s,th}$ .

## 5. Conclusions

To achieve a sustainable and efficient interconnection of diverse entities in the beyond 5G system, this study investigates the intricacies of designing transmission beams, optimizing jammer device transmission beams, and implementing phase shift designs within a SWIPT-enabled cognitive secure communication network assisted by IRS. The investigation considers the transmission power constraints of cognitive base stations and jammers, minimum security requirements for all cognitive information receiving devices, interference limitations posed by primary users, and phase shift constraints. Subsequently, we formulate a comprehensive multidimensional resource joint allocation model with objectives such as energy harvesting maximization. To address the complexity of the optimization problem, we employ a BCD method, effectively breaking it down into two distinct subproblems. The first subproblem focuses on resolving transmission beam design decisions using SCA methods. Simultaneously, the second subproblem addresses an intelligent reflective surface phase shift design and utilizes SDR methods. Extensive simulations conducted under various scenarios and conditions consistently demonstrate that the proposed approach outperforms existing solutions, highlighting its efficacy in achieving higher overall system harvested energy and prolonging the operational lifespan of the network. In future, we will explore the scenario of an IRS-aided cognitive secure transmission based on imperfect channel state information to enhance the practicality of our research.

**Author Contributions:** Y.Z. and S.L. collaboratively conceived the fundamental concept of the secure transmission scheme, conducted intricate network modeling, and executed in-depth analysis as well as comprehensive computer simulations to evaluate the proposed algorithm. Y.Z. and F.D. were responsible for drafting the manuscript. S.L. made substantial contributions by providing insightful comments and conducting a meticulous technical review of the proposed algorithm. All authors have read and agreed to the published version of the manuscript.

**Funding:** This work was supported in part by Research on The Construction of Modern Industrial Institute with The Background of “Double High Plan” under Grants 2021SJA0950, by the Qinglan Project of Jiangsu Province, by Chunhui plan international cooperation project of China Education Ministry under Grant 202201406.

**Data Availability Statement:** Data are contained within the article.

**Conflicts of Interest:** The authors declare no conflicts of interest.

## References

1. Kolodzy, P. *Spectrum Policy Task Force Report*; Federal Communications Commission: Washington, DC, USA, 2002.
2. Wong, V.W.S. *Key Technologies for 5G Wireless Systems*; Cambridge University Press: Cambridge, UK, 2017.
3. Li, X.W.; Gao, X.S.; Liu, Y.T.; Huang, G.J.; Zeng, M.; Qiao, D.W. Overlay CR-NOMA Assisted Intelligent Transportation System Networks with Imperfect SIC and CEEs. *Chin. J. Electron.* **2023**, *32*, 1258–1270.
4. Dong, Q. Spectrum Sensing Algorithm by Multi-Objective Optimization Theory and Fuzzy Integra. *IEEE Access* **2023**, *11*, 109307–109318. [[CrossRef](#)]
5. You, J.X.; Yang, G.C.; Kwong, W.C. Construction of Asynchronous Relaxed Difference Set of Q-Ary Maximum-Length Channel-Hopping Sequences for Cognitive Radio Wireless Networks. *IEEE Commun. Lett.* **2023**, *27*, 2526–2530. [[CrossRef](#)]
6. Li, Z.; Shi, J.; Wang, C.; Wang, D.Y.; Li, X.M.; Liao, X.M. Intelligent covert communication design for cooperative cognitive radio network. *China Commun.* **2023**, *20*, 122–136. [[CrossRef](#)]
7. Rehman, G.U.; Zubair, M.; Qasim, I.; Badshah, A.; Mahmood, Z.; Aslam, M.; Jilani, S.F. EMS: Efficient Monitoring System to Detect Non-Cooperative Nodes in IoT-Based Vehicular Delay Tolerant Networks (VDTNs). *Sensors* **2023**, *23*, 99. [[CrossRef](#)]
8. ur Rehman, G.; Ghani, A.; Zubair, M.; Ghayyure, S.A.K.; Muhammad, S. Honesty based democratic scheme to improve community cooperation for Internet of Things based vehicular delay tolerant networks. *Trans. Emerg. Telecommun. Technol.* **2020**, *32*, e1–e19. [[CrossRef](#)] [[PubMed](#)]
9. Yang, L.; Jiang, H.; Vorobyov, S.A.; Chen, J.; Zhang, H.L. Secure Communications in Underlay Cognitive Radio Networks: User Scheduling and Performance Analysis. *IEEE Commun. Lett.* **2016**, *20*, 1191–1194. [[CrossRef](#)]
10. Yan, P.S.; Ji, X.D.; Zou, Y.L.; Li, B. Securing Multiuser Underlay Cognitive Transmissions With Hardware Impairments and Channel Estimation Errors. *IEEE Trans. Cogn. Commun. Netw.* **2023**, *9*, 1183–1199. [[CrossRef](#)]
11. Vo, V.N.; Dang, V.H.; Tran, H.; Ha, D.B.; Le, C.; Ho, T.D.; So-In, C. Secondary Network Throughput Optimization of NOMA Cognitive Radio Networks Under Power and Secure Constraints. *IEEE Access* **2023**, *11*, 33826–33838. [[CrossRef](#)]

12. Wasilewska, M.; Bogucka, H.; Poor, H.V. Secure Federated Learning for Cognitive Radio Sensing. *IEEE Commun. Mag.* **2023**, *61*, 68–73. [[CrossRef](#)]
13. Zhu, F.C.; Yao, M.L. Improving Physical-Layer Security for CRNs Using SINR-Based Cooperative Beamforming. *IEEE Trans. Veh. Technol.* **2016**, *65*, 1835–1841. [[CrossRef](#)]
14. Lee, J.H. Full-Duplex Relay for Enhancing Physical Layer Security in Multi-Hop Relaying Systems. *IEEE Commun. Lett.* **2015**, *19*, 525–528. [[CrossRef](#)]
15. Mukherjee, M.; Shu, L.; Kumar, V.; Kumar, P.; Matam, R. Reduced out-of-band radiation-based filter optimization for UFMC systems in 5G. *IWCMC* **2015**, 1150–1155. [[CrossRef](#)]
16. Gu, Y.B.; Wu, Z.L.; Yin, Z.D.; Zhang, X.J. The Secrecy Capacity Optimization Artificial Noise: A New Type of Artificial Noise for Secure Communication in MIMO System. *IEEE Access* **2019**, *7*, 58353–58360.
17. Chi, H.R.; Radwan, A. Quality of Things' Experience for 6G Artificial Intelligent Internet of Things with IEEE P2668. *IEEE Commun. Mag.* **2023**, *58*, 58–64. [[CrossRef](#)]
18. Shao, S.J.; Zheng, J.T.; Guo, S.Y.; Qi, F.; Qiu, X.S. Decentralized AI-Enabled Trusted Wireless Network: A New Collaborative Computing Paradigm for Internet of Things. *IEEE Netw.* **2023**, *37*, 54–61. [[CrossRef](#)]
19. Ko, H.; Pack, S. OB-DETA: Observation-based directional energy transmission algorithm in energy harvesting networks. *J. Commun. Netw.* **2019**, *21*, 168–176. [[CrossRef](#)]
20. Zhang, F.; Lau, V. Delay-sensitive dynamic resource control for energy harvesting wireless systems with finite energy storage. *IEEE Commun. Mag.* **2015**, *53*, 106–113. [[CrossRef](#)]
21. Qi, Q.; Chen, X.M.; Zhong, C.J.; Zhang, Z.Y. Integration of Energy, Computation and Communication in 6G Cellular Internet of Things. *IEEE Commun. Lett.* **2020**, *24*, 1333–1337. [[CrossRef](#)]
22. Shin, J.; Shin, S.Y.; Kim, Y.S.; Ahn, S.Y.; Lee, S.W.; Jung, G.; Jeon, S.J.; Cho, D.H. Design and Implementation of Shaped Magnetic-Resonance-Based Wireless Power Transfer System for Roadway-Powered Moving Electric Vehicles. *IEEE Trans. Ind. Electron.* **2014**, *61*, 1179–1192. [[CrossRef](#)]
23. Jawarneh, A.; Kadoch, M.; Albataineh, Z. Decoupling Energy Efficient Approach for Hybrid Precoding-Based mmWave Massive MIMO-NOMA With SWIPT. *IEEE Access* **2022**, *10*, 28868–28884. [[CrossRef](#)]
24. Dang, J.; Zhang, Z.C.; Wu, L. Joint beamforming for intelligent reflecting surface aided wireless communication using statistical CSI. *China Commun.* **2020**, *17*, 147–157. [[CrossRef](#)]
25. Woo, J.; Song, C.; Lee, I. Sum Rate and Fairness Optimization for Intelligent Reflecting Surface Aided Multiuser Systems. *IEEE Trans. Veh. Technol.* **2022**, *70*, 13436–13440. [[CrossRef](#)]
26. Wu, Q.; Zhang, R. Towards Smart and Reconfigurable Environment: Intelligent Reflecting Surface Aided Wireless Network. *IEEE Commun. Mag.* **2020**, *58*, 106–112. [[CrossRef](#)]
27. Li, D. How Many Reflecting Elements Are Needed for Energy- and Spectral-Efficient Intelligent Reflecting Surface-Assisted Communication. *IEEE Trans. Commun.* **2022**, *70*, 1320–1331. [[CrossRef](#)]
28. Wu, Q.Q.; Zhang, R. Weighted sum power maximization for intelligent reflecting surface aided SWIPT. *IEEE Wirel. Commun. Lett.* **2020**, *9*, 586–590. [[CrossRef](#)]
29. Tang, Y.Z.; Ma, G.G.; Xie, H.L.; Xu, J.; Han, X. Joint transmit and reflective beamforming design for IRS-assisted multiuser MISO SWIPT systems. *IEEE Int. Conf. Commun.* **2020**, 1–6. [[CrossRef](#)]
30. Liu, J.R.; Xiong, K.; Lu, Y.; Ng, D.W.K.; Zhong, Z.D.; Han, Z. Energy efficiency in secure IRS-aided SWIPT. *IEEE Wirel. Commun. Lett.* **2020**, *9*, 1884–1888. [[CrossRef](#)]
31. Chu, Z.; Hao, W.M.; Xiao, P.; Shi, J. Intelligent reflecting surface aided multi-antenna secure transmission. *IEEE Wirel. Commun. Lett.* **2020**, *9*, 108–112. [[CrossRef](#)]
32. Wang, H.M.; Bai, J.L.; Dong, L.M. Intelligent Reflecting Surfaces Assisted Secure Transmission Without Eavesdropper's CSI. *IEEE Signal Process. Lett.* **2020**, *7*, 1300–1304. [[CrossRef](#)]
33. Yu, X.H.; Xu, D.F.; Sun, Y.; Ng, D.W.K.; Schober, R. Robust and secure wireless communications via intelligent reflecting surfaces. *IEEE J. Sel. Areas Commun.* **2020**, *38*, 2637–2652. [[CrossRef](#)]
34. Cho, Y.Y.; Lee, J.H.A. New Cooperative Jamming Technique for a Two-Hop Amplify-and-Forward Relay Network With an Eavesdropper. *IEEE Trans. Veh. Technol.* **2020**, *67*, 12447–12451. [[CrossRef](#)]
35. Liu, C.; Liu, X.M.; Ng, D.W.K.; Yuan, J.H. Deep Residual Learning for Channel Estimation in Intelligent Reflecting Surface-Assisted Multi-User Communications. *IEEE Trans. Wirel. Commun.* **2022**, *21*, 898–912. [[CrossRef](#)]

**Disclaimer/Publisher's Note:** The statements, opinions and data contained in all publications are solely those of the individual author(s) and contributor(s) and not of MDPI and/or the editor(s). MDPI and/or the editor(s) disclaim responsibility for any injury to people or property resulting from any ideas, methods, instructions or products referred to in the content.